Effects of thermomechanical history on the tensile behavior of Nitinol ribbon

Cynthia L. Lach[*a], Travis L. Turner[**a], Karen M. Taminger[***a] and Ravi N. Shenoy[****b]
[a]NASA Langley Research Center; [b]Lockheed Martin

ABSTRACT

Shape memory alloys (SMAs) have enormous potential for a wide variety of applications. A large body of work exists on the characterization of the microstructure and stress-strain behavior of these alloys, Nitinol (NiTi) in particular. However, many attributes of these materials are yet to be fully understood.

Previous work at NASA Langley Research Center (LaRC) has included fabrication of hybrid composite specimens with embedded Nitinol actuators and modeling of their thermomechanical behavior. An intensive characterization effort has been undertaken to facilitate fundamental understanding of this alloy and to promote implementation of Nitinol in aerospace applications. Previous work revealed attributes of the Nitinol ribbon that were not easily rationalized with existing data in the literature. In particular, tensile behavior at ambient temperature showed significant dependence on the thermomechanical history prior to testing. The present work is focused on characterizing differences in the microstructure of Nitinol ribbons exposed to four different thermomechanical histories and correlation of the microstructure with tensile properties. Differential scanning calorimetry (DSC) and x-ray diffraction (XRD) analysis were employed to rationalize the microstructures present after exposure to various thermomechanical histories. Three of the Nitinol ribbon conditions were reversible upon heating (in the DSC) through the reverse transformation temperature (A_f) to transform the microstructure to austenite. However, the prior thermomechanical conditioning for the Nitinol ribbon that reflected the entire fabrication procedure (4% thermal cycle condition) was found to have an irreversible effect on the microstructure, as it remained unchanged after repeated complete thermal cycles.

Tensile tests were conducted to determine the effect of prior thermomechancial conditioning on both the tensile behavior of the Nitinol ribbons and the stress state of the microstructure. The stress-strain behavior of the Nitinol actuators appears to be governed by the interplay between two major variables: namely, microstructural constituents such as the R-phase and the martensite; and the stress state of these constituents (whether twinned with low residual stresses, or detwinned with high residual stresses). The most significant difference in the stress-strain behavior of the four conditions, the critical stress required to achieve an initial stress plateau, was found to depend on both the amount and stress state (twinned or detwinned) of R-phase present in the initial microstructure. Thus, the effect of prior thermomechanical processing is critical to the resulting tensile behavior of the Nitinol actuator. For numerical modeling inputs one must take into account the entire fabrication process on the Nitinol actuator.

Key Words: shape memory alloys, Nitinol, NiTi, microstructure, stress-strain behavior, XRD, DSC

1. INTRODUCTION

Nitinol, a shape memory alloy developed in 1958 at the Navy Ordnance Laboratory, is composed of approximately 50-50 atomic percent nickel and titanium[1]. The alloy's shape memory effect (SME) can be thermally and/or stress-induced[2]. SMAs exhibit desirable attributes that have substantial potential for a variety of aerospace applications[2]. Because of the strong application potential, a significant amount of work has been done in recent years to exploit these behaviors. Recent work at NASA LaRC has involved fabrication of hybrid composite specimens with embedded Nitinol SMA actuators, thermomechanical property characterization of the individual constituents of the material system,

[*] c.l.lach@larc.nasa.gov; phone 757 864-3133; fax 757 864-7893; http://www.larc.nasa.gov; NASA Langley Research Center (LaRC), Metals and Thermal Structures Branch, Mail Stop 188A, Hampton, VA, USA 23681-2199; [**]t.l.turner@larc.nasa.gov; phone 757 864-3598, fax 757 864-8823; http://stab.larc.nasa.gov; NASA LaRC, Structural Acoustics Branch, Mail Stop 463, [***]k.m.taminger@larc.nasa.gov; phone 757 864-3131; fax 757 864-7893; NASA LaRC, Metals and Thermal Structures Branch; [****]r.n.shenoy@larc.nasa.gov; phone 757 864-8723, fax 757 864-7893; Lockheed Martin, Hampton, VA, 23662

SPIE's 9th Annual International Symposium on Smart Structures and Materials; Active Materials: Behavior and Mechanics, Christopher S. Lynch (Editor), SPIE Vol. 4699, Paper No. 4699-45, San Diego, CA, 17-21 March 2002.

testing of the hybrid composite specimens for static and dynamic responses, and correlation of the measured responses with the prediction of numerical models[3-4]. Although the overall features of any process to fabricate a composite with embedded SMA actuators may appear similar, there is the opportunity for a multitude of permutations that can affect the thermomechanical history of the SMA actuators. It is important to note that differences in thermomechanical history not only affect the SMA actuator performance, but also affect the manner in which materials testing must be conducted to provide data for numerical models.

One such processing and fabrication approach used to produce SMA hybrid composites (SMAHC) at NASA LaRC is described in previous reports[3-4]. Essential components of the process include removal of "packaging" strain induced in the SMA during spooling by the vendor, axial elongation of the SMA actuators, embedding of the SMA actuators within a composite matrix, and constraint of the SMA actuators during an autoclave cure cycle. The thermomechanical properties of these SMAHCs were determined from tests performed on the constituents at various temperatures ranging from ambient to 149°C (300°F). However, correlation of measured and predicted static and dynamic responses of the specimens showed some discrepancies. Investigation into sources for the discrepancies included further tensile testing of Nitinol samples after subjecting the samples to a constrained thermal cycle, which was intended to simulate the conditions of the autoclave cure cycle. Substantial differences were found in the tensile behavior of pre-strained samples that were subjected to the constrained thermal cycle versus those that were not[3]. The present study is, therefore, aimed at understanding why these differences in mechanical property behavior exist and to explore whether there is an optimal microstructural condition for the Nitinol actuators prior to embedding them in the hybrid composite. Such a study, it is believed, may help in improving the accuracy of the numerical models, and also contribute to the development of a manufacturing process for the SMAHC specimens with improved performance of the SMA actuators.

2. BACKGROUND

Nitinol ribbon (0.226 cm wide by 0.0163 cm thick), with a nominal composition of 55.4Ni-44.3Ti (atomic percent, balance: C, O, H, N, and Fe impurities) was obtained from Shape Memory Applications, Inc. The nominal transformation temperatures reported earlier[3] for this alloy are M_s=46°C, M_f=32°C, A_s=67°C, and A_f=86°C, where M_s and M_f refer to start and finish temperatures for the austenite to martensite transformation during cooling, similarly, A_s and A_f are the start and finish temperatures for the martensite to austenite transition during heating. As mentioned previously, the first step in the fabrication process employed at NASA LaRC involved the removal of the packaging strain. This was done by resistively heating the Nitinol ribbons to ~149°C for less than a minute while the ribbon was held by a minimum of constraint, followed by conventional air cooling to ambient temperature[3]. After the removal of the packaging strain, the material is now said to be in the "recovered" state. Three additional material conditions were also studied, the recovered frozen, 4%, and 4% thermal cycle conditions. Each of these conditions used recovered material as a precursor. Material in the recovered frozen condition was produced by quenching recovered material in liquid N_2 to ensure the formation of 100% twinned martensite (i.e. martensite formed during cooling below M_f in the absence of stress). Material in the 4% condition was pre-strained to 4% total elongation. The 4% thermal cycle condition was produced by straining material to 4% elongation and thermally cycling from room temperature to 149°C and cooling back to room temperature, while the material was constrained. The 4% thermal cycle condition is consistent with the thermomechanical processing experienced by the embedded Nitinol ribbon actuators in the SMAHC produced at NASA LaRC. The final thermal cycling step with the material constrained simulates the autoclave cure cycle experienced by the embedded SMA actuators.

Nitinol ribbon samples in the above four conditions were subjected to x-ray diffraction, differential scanning calorimetry and tensile tests to identify the phases present as a function of temperature and applied strain. The tensile and XRD tests were conducted at ambient temperature.

3. RESULTS AND DISCUSSION

3.1 Nitinol XRD Characterization

The Nitinol ribbon samples in the recovered, 4%, and 4% thermal cycle conditions were scanned over the 2θ range of 10°-125° in a Siemens D5000 x-ray diffractometer. A position sensitive detector was used in conjunction with a Cu

target, with the x-ray tube operated at 45kV / 40 mA. Figure 1 shows the XRD results in the 2θ range of 20°-80°. Three specific phases of NiTi are identified for charaterization: martensite (M), austenite (A), and R-phase (R). Additional details of these phases are listed in Table 1. A positive identification was made of the martensite phase based on the International Centre for Diffraction Data (ICDD). The R-phase formation in Nitinol alloys has often been referred to as a rhombohedral distortion of the austenite [5], resulting in nearly equivalent d-spacings for the austenite and R-phase. Consequently, x-ray reflections are expected to be observed at nearly the same values of 2θ. Additionally, standard x-ray reflection peaks for the R-phase are not supplied in the ICDD database. This makes an unequivocal distinction of austenite and R-phase using x-ray diffraction, impractical. Due to the similarity of the austenite and R-phase, a convenient description of the β phase as being a structure encompassing both austenite and the R-phase has been presented.[6] An unambiguous identification of solely the R-phase (as opposed to austenite) will be shown in the DSC characterization section. The Nitinol ribbons had significant crystallographic texture, as evidenced by the lack of conformity of the observed integrated intensities of the x-ray reflections for the various phases with those reported for these phases in the ICDD database. Other uncertainty in the XRD data exists due to the difficulty deconvoluting multiple high intensity peaks.

Table 1. Crystallographic Properties of Phases Present in Nitinol Ribbon.

Abbreviation	Phase	Crystallographic Structure	X-ray Reflections	ICDD
			Peak Intensity (%)	2θ (degrees)
M	B19'	martensite, monoclinic (distortion of B19)	65 80 55 100	39.135* 41.384* 43.906* 45.070*
A	B2	austenite, CsCl structure	100 40 60 10	42.793* 61.979* 78.151* 93.334*
R	R-phase	martensite, rhombohedral/trigonal (distortion of austenite)	+ + +	+ + +

*Values from ICDD: martensite ICDD 27-0344, austenite 18-0899
+Not included in ICDD[6]

3.2 Nitinol DSC Characterization

DSC tests were conducted on samples in the four alloy conditions to characterize the phase transitions involving the M, R and A phases during heating and cooling. The positions of the R_s, R_f, M_s, and M_f temperatures relative to ambient temperature give an indication of R-phase and martensite volume fractions at ambient temperature. Here, R_s and R_f denote the start and end of the A → R transition, during cooling. The sequence of reactions, in addition to the transformation temperatures, is influenced by prior thermomechanical history of the alloy. For example, cold working followed by annealing within the temperature regime of 360°C-660°C (when originally producing the Nitinol ribbon) can give rise to the following sequence of reactions[7].

low temperature heat treatment ⇒ A → R → M (during cooling)
⇒ M → R → A (during heating)

intermediate temperature heat treatment ⇒A → R → M (during cooling)
⇒M → A (during heating)

high temperature heat treatment ⇒ A → M (during cooling)
⇒ M → A (during heating)

In addition to the above general sequence of possible reactions within the NiTi system, during cooling or heating, the transformation temperatures can themselves be modified by the application of an external stress[8] and/or by thermal cycling[9].

Samples with each of the four alloy conditions were subjected to a series of cooling/heating steps in the DSC, to characterize their microstructures and the associated transformation temperatures, see Table 2. A maximum temperature of 100°C was determined to be well above the temperature required to obtain a fully austenitic condition for each of the four alloy conditions. The first cooling cycle (step 1) was conducted to determine if any residual A or R-phase was present in the ambient microstructure. Cooling to -30°C leads to the transformation of the residual A or R-phase into martensite, with the area under this exotherm being a measure of the volume fraction of the residual phase. The first heating cycle (step 2) was meant to register the signatures of the M → A transformation, in addition to possible M → R and R → A reactions. The second cooling cycle (step 3) had the objective of recording the characteristics of the sequential A → R and the R → M transformations. In addition, the second cooling cycle has the potential of revealing the stress state of the transforming A, via the relative positions of the R_s, R_f, M_s, and M_f temperatures. The second heating cycle (step 4) is intended to detail the M → A transition together with those of the other plausible reactions. In addition, the second heating cycle might reveal whether repeated heating of an ambient/sub-ambient microstructure has any effect in erasing the influence of prior thermomechanical history on a resulting microstructure. Samples of the recovered and 4% thermal cycle conditions were subjected to three additional thermal cycles (steps 5 through 7), to determine the microstructural stabilities for these thermomechanical histories. The results of the DSC tests, presented in Figures 3 through 6, show the various reactions for steps 1 through 4. The transformation temperatures for the martensite, R-phase, and austenite are shown in Table 3 for steps 1 through 4 and in Table 4 for steps 5 through 7. The area under the curve per unit sample mass was determined for each transformation to indicate the relative amount of the phase/phases present in the microstructure. The calculated area for martensite, R-phase, and austenite are shown in Table 5.

Table 2. Heating/Cooling Sequences for DSC Testing.

Step	Procedure	Temperature Range (°C)	Ramp Rate (°C/min)
1	1st cooling	ambient to -30°C	5
2	1st heating	-30°C to 100°C	5
3	2nd cooling	100°C to -30°C	5
4	2nd heating	-30°C to 100°C	5
5*	3rd cooling	100°C to -30°C	5
6*	3rd heating	-30°C to 100°C	5
7*	4th cooling	100°C to -30°C	5

*Only the recovered and 4% thermal cycle samples were subject to steps 5-7.

The initial cooling cycle for both the recovered and 4% thermal cycle conditions reveals a single exotherm representing either the A → M or the R-phase → M reaction (see Figures 2 and 5). M_s was ~14.6°C for the recovered condition versus 13.6°C for the 4% thermal cycle condition. The corresponding M_f for the two conditions were 2.5°C versus ~0.9°C (see Table 3). For these two conditions, the initial microstructure is comprised of either A or the R-phase in addition to M. Whether the initial microstructure contains A or the R-phase would be dictated by the location of the R_f (to be determined from step 3) relative to ambient temperature. During the first cooling, the martensite exotherm is not observed for the recovered frozen or 4% conditions. This suggests that all of the martensite that can be generated by cooling or stress was produced during the initial thermomechanical processing. For the recovered frozen condition, the liquid nitrogen quench results in the formation of twinned martensite (i.e. formed during cooling below M_f in the absence of stress). In the 4% condition, the 4% pre-strain resulted in the transformation of the mixture of austenite + R-phase to detwinned martensite (formed after reaching the critical stress $\{\sigma_{ms}\}$ required to reorient martensite).

The first heating cycle for all four alloy conditions was characterized by the presence of an asymmetric endothermic peak (see Figures 2-5). The endotherm is complex for both the 4% and 4% thermal cycle conditions. The asymmetry and/or the complex nature of the endotherm suggests the possible occurrence of three plausible concurrent reactions, viz. M → R, R →A, and M→ A (in that order) [7]. The 4% condition is characterized by a significantly narrower A_s-A_f range

(~1.9°C) together with a significantly higher peak temperature (67.7°C) than for the other three conditions (see Table 3). Similar results[7, 11] have been used to suggest that the narrow endothermic peak is a result of limited martensite variants present. While undeformed Nitinol alloys can contain 24 variants[10], the prior deformation appears to have reduced the number of twinned martensite variants. With limited martensite variants present, the transformation of martensite to

Table 3. Transformation Temperatures as a Function of Thermal History (steps 1-4).

Condition	1st Cool (step1)		1st Heat (step 2)		2nd Cool (step 3)				2nd Heat (step 4)	
	M_s	M_f	A_s	A_f	R_s	R_f	M_s	M_f	A_s	A_f
Recovered	14.61°C	2.48°C	53.25°C	62.25°C	45.08°C	39.13°C	20.61°C	6.30°C	53.58°C	61.19°C
Recovered Frozen	----------	----------	54.77°C	63.46°C	44.97°C	39.13°C	20.94°C	6.24°C	53.74°C	61.51°C
4%	----------	----------	66.94°C	68.83°C	45.18°C	39.56°C	20.77°C	6.25°C	53.88°C	60.55°C
4% Thermal Cycle	13.65°C	0.93°C	51.25°C	64.68°C	50.31°C	36.35°C	16.52°C	1.15°C	51.60°C	62.01°C

Table 4. Transformation Temperatures as a Function of Thermal History (steps 5-7).

Condition	3rd Cool (step 5)				3rd Heat (step 5)		4th Cool (step 7)			
	R_s	R_f	M_s	M_f	A_s	A_f	R_s	R_f	M_s	M_f
Recovered	45.06°C	39.14°C	20.31°C	6.21°C	53.68°C	61.17°C	45.05°C	39.17°C	20.15°C	6.02°C
4% Thermal Cycle	49.86°C	36.44°C	16.12°C	0.85°C	51.72°C	61.85°C	49.62°C	36.55°C	15.80°C	0.91°C

Table 5. Enthalpies for Transformation of Phases as a Function of Thermal History.

Condition	1st Cool (step1)	1st Heat (step 2)	2nd Cool (step 3)		2nd Heat (step 4)	3rd Cool (step 5)		3rd Heat (step 6)	4th Cool (step 7)	
	M	A	R-phase	M	A	R-phase	M	A	R-phase	M
Recovered	-2.08 J/g	22.22 J/g	-6.29 J/g	-13.62 J/g	23.02 J/g	-6.23 J/g	-13.46 J/g	23.22 J/g	-6.043 J/g	-13.44 J/g
Recovered Frozen	---------	21.31 J/g	-5.90 J/g	-12.63 J/g	22.61 J/g	---------	---------	---------	---------	---------
4%	---------	22.99 J/g	-5.63 J/g	-12.95 J/g	21.97 J/g	---------	--------	---------	---------	---------
4% Thermal Cycle	-4.23 J/g	18.90 J/g	-3.78 J/g	-9.30 J/g	19.28 J/g	-3.78 J/g	-9.94 J/g	19.47 J/g	-3.70 J/g	-9.80 J/g

austenite and/or R-phase will occur over a much finer range of temperature than will be observed if many martensite variants are present. For the 4% thermal cycle condition, the widest observed A_s-A_f temperature range of ~13.4°C was apparent, as indicated in Table 3. Because of the complex stress state of this alloy condition, it is likely that the 100% martensite microstructure obtained at the end of the first cooling cycle may indeed have a partly thermoelastic character and a partly stress-induced character to it. The decomposition of such a martensite mixture during the first heating cycle can then be expected to result in a more complex endotherm, such as that obtained in the present study (see Figure 5). The complex residual stress state of the 4% thermal cycle condition may be responsible for the coexistence of the R-phase + martensite over a wider temperature range. At the end of the first heating cycle (100°C), the microstructure in each of the four conditions consists entirely of the austenite phase.

During the second cooling cycle, all four thermomechanical conditions were typified by the A $\rightarrow$ R and R $\rightarrow$ M sequence of exothermic reactions (see Figures 2-5). The R_s for the 4% thermal cycle condition was the highest (50.3°C) among the four alloy conditions, with R_s being essentially similar for the recovered, the recovered frozen, and the 4% conditions (~45°C) (see Table 3). R_f for the 4% thermal cycle condition was lower (36.4°C) than the ~39°C R_f observed

for the three other conditions (see Table 3). The R_s-R_f range was nearly 14°C for the 4% thermal cycle condition, yet was less than 6°C for the three other conditions. The M_s (16.5°C) and M_f (1.2°C) temperatures for the 4% thermal cycle condition were the lowest among the four alloy conditions. The Ms (~20.8°C), and M_f (~6.2°C) were similar for the other three conditions (see Table 3). Not only were the (R_s, R_f) and (M_s, M_f) similar in the recovered, the recovered frozen, and the 4% conditions, but so were the R-phase and martensite volume fractions for these conditions (see Table 5). This strongly suggests that the first heating cycle, which preceded this second cooling, effectively removes the prior deformation influence on the subsequently evolving microstructures in the 4% condition. As a result, the 4% condition is microstructurally similar to the recovered and the recovered frozen conditions subsequent to the first heating cycle. In contrast, the R-phase (3.78 J/g) and martensite (9.30 J/g) volume fractions in the 4% thermal cycle condition were substantially different, than for the other conditions (see Table 5). The higher R_s, lower R_f, greater (R_s-R_f) range, and lower M_s and M_f temperatures, observed for the 4% thermal cycle condition during the second cooling cycle are in agreement with the literature[8, 11], in so far as the effects of residual stresses on the A → R and R → M transformation characteristics are concerned. The first heating cycle did not eliminate the built-in residual stresses produced by the thermomechanical history applied to the 4% thermal cycle condition. Stresses induced in the austenite during cooling, either by mechanical deformation (such as that in the 4% thermal cycle condition) or through precipitation of coherent $TiNi_3$ precipitates, are known to promote earlier R-phase formation, and also suppress R-phase conversion into M to lower temperatures[12]. The A → R transformation is observed for all four alloy conditions in the second cooling cycle. Additionally, it can be seen that this transformation is complete at temperatures above room temperature. Consequently, austenite will not be present in any of the thermomechanical conditions. Significantly lower exothermic heats for the A → R (3.78 J/g) and R → M (9.30 J/g) transitions were observed for the 4% thermal cycle condition (see Table 5). This is most likely due to the unrelieved stresses in austenite (which were caused by the 4% deformation of the austenite when the sample was constrained during heating) alter the temperature characteristics of the R-phase and martensite reactions during the subsequent cooling, but they also inhibit the release of exothermic heats during the A → R and R → M transitions. In contrast, the A → R exothermic heats were very similar (~6 J/g) in the recovered, the recovered frozen, and the 4% conditions; as were the corresponding R → M exothermic heats for these conditions (~13 J/g).

The second heating cycle was conducted to see if a repeated heating cycle had any significant effect on the transformational characteristics of the various alloy conditions. At the end of the first heating cycle for the 4% condition, the prior deformation appeared to be almost completely removed. This conclusion is supported by similar A_s (~54°C) and A_f (~61°C) temperatures for the 4%, the recovered, and the recovered frozen conditions during the second heating cycle (see Table 3). In contrast, the 4% thermal cycle condition, which exhibits a relatively high A_f and a relatively low A_s temperature and a large A_s-A_f temperature differential during the first heating cycle was largely unaffected by the repetitive heating cycles in the DSC (see Table 3). This suggests that residual stresses resulting from the prior deformation and constrained thermal cycling treatment remain in the microstructure.

The recovered and 4% thermal cycle conditions were subjected to additional heating-cooling cycles to document the microstructural stabilities for these two conditions. For both alloy conditions, the A_s, and the A_f temperatures are nearly the same for the 2nd and 3rd heating cycles. Similarly, the R_s, R_f, M_s, and M_f temperatures during the 3rd and the 4th cooling cycles were similar to those recorded during the 2nd cooling cycle. This clearly implies that once the first heat cycle has been applied, the subsequent heating-cooling cycles do not alter the alloy microstructures. Also, the exothermic heats associated with the A → R and R → M transitions were consistent during the 2nd, 3rd, and 4th cooling cycles (see Table 5). The exothermic heat for the A → R transition in the recovered condition was substantially larger than was observed for the 4% thermal cycle condition (see Table 5). Similarly, exothermic heat for the R → M transition in the recovered condition was significantly larger than was observed for the 4% thermal cycle condition (see Table 5). For a given alloy condition, the ratio (R → M exotherm): (A →R exotherm), termed α, provides a quantitative basis for the heat effects associated with the production of 100% martensite and 100% R-phase in the alloy. The difference in the values of α for the recovered versus the 4% thermal cycle condition may then be related to the nature of the martensite and the R-phase in these alloy conditions. For example, α is ~18% higher in the 4% thermal cycle condition than in the recovered condition for the 2nd, 3rd, and 4th cooling cycles (see Figure 6). The 4% thermal cycle condition was distinguished by the presence of high levels of residual stresses. In comparison, the recovered condition is expected to be relatively stress-free. Values of α for the two alloy conditions may therefore be viewed as prominent indicators of stress states of the R-phase and the martensite in these alloys.

Based on the above DSC data for the first cooling and the second cooling cycles, the initial microstructure for the four thermomechanical conditions can be determined from the volume fraction of phases shown in Table 5. Both the recovered and 4% thermal cycle conditions contained R-phase (2.08 J/g and 4.23 J/g, respectively) at ambient temperature. In addition, martensite (as given by the martensite area during second cooling cycle (step 3.) minus the martensite area during first cooling cycle (step 1.) due to R-phase conversion) was also present in these two conditions, with respective areas being 11.54 J/g and 5.07 J/g. In contrast, the 4% condition contained only the martensite phase (12.95 J/g, based on step 3.). Based on the DSC results, the relative volume fractions of M and R-phase present in the four alloy conditions were determined and are presented in Figure 7. If the microstructure prior to the 4% pre-strain (i.e., the recovered condition) was dominated by the presence of R-phase, the post-deformation microstructure is likely to have a larger volume fraction of detwinned martensite. This is because R $\rightarrow$ M conversion is facilitated by cold work[12]. Indeed, the higher martensite content in the 4% condition is evidenced by both XRD and DSC results in the present study. The recovered frozen condition on the other hand, would result in 100% twinned martensite. In brief, the initial microstructures for the four alloy conditions are:

Recovered $\Rightarrow$ (twinned R-phase + twinned martensite) mixture with low residual stresses
Recovered frozen $\Rightarrow$ ~100% twinned martensite, with low residual stresses
4% $\Rightarrow$ ~100% detwinned martensite, with significant residual stresses
4% thermal cycle $\Rightarrow$ (detwinned R-phase + detwinned martensite) mixture with high residual stresses

Based on the sequence of phase transformations apparent in the first and the second cooling cycles, the Nitinol ribbon in the as received condition (prior to its being utilized for producing the four alloy conditions) was most likely subjected to a low temperature heat treatment (~330-410°C) [7] during its fabrication.

3.3 Nitinol Stress-Strain Behavior

Tensile behavior for Nitinol ribbon samples in each of the four alloy conditions was characterized. The 4% and the 4% thermal cycle conditions were obtained by pre-straining individual 0.635 m long recovered Nitinol ribbons to 4 percent total elongation, at a strain rate of 6.35 m/min. A typical stress-strain curve for the pre-straining procedure is shown in Figure 8. Ambient tensile tests for all four conditions were conducted on ribbons with a 0.127 m long gage length, at a constant cross head speed of 0.127 m/min, according to ASTM E8-00[13]. The stress-strain behavior for each condition is shown in Figure 9. Figure 9 (a) shows the initial stress-strain curve while Figure 9 (b) shows the entire tensile behavior for all four alloy conditions.

The character of the stress-strain curve for a given sample condition is dictated by the initial microstructure of the sample; (i.e., the relative volume fractions of the R-phase and the martensite), the stress state of these two phases, and the residual stresses induced in the microstructure either by prior mechanical deformation of the austenite or through precipitation of coherent $TiNi_3$ precipitates[12]. The manner in which the microstructural differences affect the tensile behavior will be described in the following discussion.

A generalized tensile curve depicting the behavior of Nitinol alloy with a 100% twinned martensite has been developed[2, 14-15] (see Figure 10). Within region I of the stress-strain curve, elastic accommodation of the martensite twins with an initial modulus E_i. Region II, typified by a near constant stress plateau, σ_{ms}, has been related to the reorientation of martensite twins. This process has also been termed detwinning, and it continues throughout region II until the critical finish stress level σ_{mf}, where a single variant of martensite is obtained[14]. In region III, the linear elastic response E_s of the fully detwinned martensite is observed. At the end of region III, the plastic flow stress σ_p is reached. Upon further deformation into region IV, a second stress plateau is observed which is related to increasing slip and dislocation movement within the microstructure. Region IV is thus characterized by plastic deformation of the detwinned martensite until fracture occurs at the stress value of σ_f. Prior thermomechanical histories of the alloy, such as those studied in the present investigation are expected to influence these four stages of stress-strain behavior. It is known that the stress needed to detwin R-phase and subsequently promote the conversion of detwinned R-phase into detwinned martensite is very low compared to that needed to detwin twinned martensite[16].

The tensile behavior of the recovered frozen condition, having no pre-strain, should most closely resemble that described in Figure 10. However, there are notable differences between the tensile behavior of the recovered frozen condition (see Figure 9) and the idealized representation. In particular, there are extended regions of transition for the recovered frozen condition between regions I and II, regions II and III, and regions III and IV. These transition regions are believed to result from a mixture of micromechanical effects. For example, the transition between regions I and II may result from a simultaneous occurrence of elastic deformation of the twinned martensite variants and the onset of detwinning. The region II-III transition is expected to consist of linear elastic deformation of martensite twin variants already detwinned in the load-preferred direction and continued reorientation of martensite variants that are more reluctant to move. Likewise, the onset of plasticity is accompanied by continued but diminishing elastic deformation of detwinned martensite, which results in the region III-IV transition common to all of the samples.

The stress-strain curve shown in Figure 8 is for a specimen with no prior deformation (i.e. recovered condition). Thus the tensile behavior observed up to 4% elongation is equivalent to that of the recovered ribbon strained up to 4% in Figure 9a. This is because the conditions are analogous. Futhermore, it can be seen by comparing the pre-strain stress-strain behavior of the recovered condition in Figure 8 with the initial portion of the tensile behavior for the 4% condition in Figure 9a that the latter's behavior is essentially a continuation of the former's. More specifically, the 4% condition (viz.~100% substantially detwinned martensite) deforms elastically until enough stress is generated to continue reorientation of the more adverse martensite variants. Note the inherent strengths of the microstructures at low strain as indicated by the critical stress at initiation of region II of the four conditions, with the following decreasing order: 4%, recovered frozen, recovered, and 4% thermal cycle. This is in agreement with the relative amounts of and condition of R-phase content in the respective microstructures as described in the DSC section and affords the following hypothesis for the respective deformation processes up to the region II-III transition. The 4% condition is the most reluctant to deform because it is already ~100% substantially detwinned martensite and deforms as described above. The recovered frozen condition is ~100% twinned martensite, which is more difficult to reorient than R-phase is to deform and/or transition to martensite and deforms primarily by martensite reorientation. Both the recovered and 4% thermal cycle conditions have a mixed microstructure of R-phase and martensite. However, based on the initial cooling cycle, the DSC results indicate that the recovered condition has roughly twice the martensite content of the 4% thermal cycle condition. The lower R_s temperature and the smaller R_s-R_f temperature range observed for the recovered condition indicates that the R-phase in the recovered condition is significantly less stressed than in the 4% thermal cycle condition. Thus it is anticipated that the stress-strain behavior of the recovered condition consists of R-phase deformation and transformation to twinned martensite. The 4% thermal cycle condition transforms to detwinned martensite more readily because of stresses already present in the microstructure. Also, note that the 4% thermal cycle condition moves into region II-III transition rather quickly due to deformation already in the microstructure, analagous to the 4% condition. Finally, the deformation behavior of all conditions is similar above their respective region II terminations because the same process is governing namely martensitic reorientation and linear elastic deformation of detwinned martensite.

It can be seen from the above discussions that the thermomechanical properties of Nitinol actuators are highly dependent upon thermomechanical history. This fact is of particular significance for developing numerical models and/or optimizing the condition of the SMA actuators for particular applications. For example, a fabrication process that subjected the Nitinol actuators to various thermomechanical treatments motivated the definition of the four alloy conditions in the Background section. One would be grossly in error to model the small stress-strain elastic behavior of such a SMAHC laminate using a modulus estimate for Nitinol from the 4% condition.

4. SUMMARY AND CONCLUSIONS

Samples of the Nitinol material in various conditions at ambient temperature were subjected to unconstrained thermal cycles in a DSC analyzer. The thermal cycles were initiated by cooling from ambient temperature first in order to determine if any residual A or R-phase was present in the ambient microstructures. Typically upon first heat the removal of reversible microstructural differences occurs by inducing the transformation to the unique miscrostructure of austenite. It was found that these repetitive unconstrained cooling-heating cycles in the DSC analysis on the recovered, recovered frozen, and 4% alloy conditions did bring about similar microstructures with similar transformational characteristics. On the other hand, repetitive unconstrained cooling-heating cycles of the 4% thermal cycle condition showed characteristics that were very different than the three other conditions. For this condition, the R-phase formed

not only earlier but also over a much wider temperature range than for the other three conditions; also, the M_s and M_f temperatures for this condition were lower. These temperature-related data suggest that the 4% thermal cycle condition had appreciable levels of residual stresses. Both the R-phase and the martensite in the 4% thermal cycle condition could be expected to be largely in the detwinned state.

Exothermic heats related with conversion of austenite into 100% R-phase and conversion of this R-phase into 100% martensite were significantly different for the recovered condition versus the 4% thermal cycle condition. These differences appeared to depend on the stress states of the two alloy conditions. For example, on a relative scale ~18% higher thermal energy was needed in the 4% thermal cycle condition to transform 100% R-phase into 100% martensite, than in the recovered condition (see Figure 7). The near constancy of this difference for the multiple cooling cycles once again attests to the high stability of the microstructures in these thermomechanical conditions. On an absolute scale however, higher thermal energies were associated with the A $\rightarrow$ R and R $\rightarrow$ M transitions in the recovered condition than in the 4% thermal cycle condition.

Based on DSC and stress-strain analysis, the ambient microstructures of the various thermomechanical conditions are rationalized to be the following:
Recovered $\Rightarrow$ (twinned R-phase + twinned martensite) mixture with low residual stresses
Recovered frozen $\Rightarrow$ ~100% twinned martensite, with low residual stresses
4% $\Rightarrow$ ~100% detwinned martensite, with significant residual stresses
4% thermal cycle $\Rightarrow$ (detwinned R-phase + detwinned martensite) mixture with high residual stresses

The stress-strain behavior of Nitinol actuators appears to be governed by the interplay between two major variables, namely, microstructural constituents such as the R-phase and the martensite: and stress state of these constituents (whether twinned with low residual stresses, or detwinned with high residual stresses). Consequently, the most significant differences in the stress-strain behavior of the four conditions occur at low stress levels, and are substantially characterized by the critical stress to induce the initial plateau (the region II). It is believed that this is governed by the respective R-phase content and condition in the microstructure. The recovered frozen condition deforms predominantly by martensite reorientation. The recovered condition, having a mixture of predominantly twinned R-phase and twinned martensite, exhibits a lower critical stress due to R-phase deformation and transformation to detwinned martensite. The 4% thermal cycle condition also possesses a mixed R-phase and martensite microstructure, but it is substantially stressed and thus deforms primarily by transformation to detwinned martensite as aided by the residual stresses. The 4% condition exhibits the highest critical stress of all because its microstructure is ~100% detwinned martensite, so enough stress must be developed in the material during testing to continue reorientation. These results demonstrate the enormous effect that a seemingly innocuous process may have on SMA actuators. This effect is of particular importance for modeling and/or optimizing actuators for specific applications.

ACKNOWLEDGEMENTS

The authors gratefully acknowledge the assistance of Joel Alexa, Stewart Walker, and Harold Claytor (Lockheed Martin) for their help in conducting the X-ray and tensile tests of the Nitinol ribbons. Thanks are also due to Crystal Topping (NASA LaRC) for her assistance in providing differential scanning calorimetry measurements from the Nitinol ribbons. Thanks are also due to Susanne Waltz (NCI Information Systems) for her assistance in reproducing the DSC thermogram figures.

REFERENCES

1. W. B. Cross, A. H. Kariotis, and F. J. Stimler, "Nitinol Characterization Study," NASA CR-1433, pp.1-60, 1969.
2. T.W. Duerig, K.N. Melton, D. Stockel, and C.M. Wayman,, *Engineering Aspects of Shape Memory Alloys*, "An Introduction to Martensite and Shape Memory", pp. 3-20, T. W. Duerig, K. N. Melton, D. Stockel, and C. M. Wayman (Editors), Butterworth-Heinemann, Boston, 1990.

3. T. L. Turner, C. L. Lach, and R. B. Cano, "Fabrication and characterization of SMA hybrid composites," Smart Structures and Materials 2001: *Active Materials: Behavior and Mechanics*, SPIE 4333-60, pp. 343-354, Newport Beach, CA, 2001.
4. T. L. Turner, "Experimental validation of a thermoelastic model for SMA hybrid composites," Smart Structures and Materials 2001: *Modeling, Signal Processing, and Control in Smart Structures*, SPIE 4326-24, pp. 208-219, Newport Beach, CA, 2001.
5. H. C. Ling and R. Kaplow, "Stress-induced shape changes and shape memory in the R and martensite transformations in equiatomic NiTi ", *Metallurgical Transactions A*, **11A**, pp. 77-83, 1980.
6. K. Otsuka and X. Ren, "Martensitic transformations in noferrous shape memory alloys*", Materials Science and Engineering*, **A273-275**, pp. 89-105, 1999.
7. T. Todoroki and H. Tamura, *Transactions of the Japan Institute of Metals*, **28**, No.2, pp. 83-94, 1987.
8. W. Huang and Y.L. Wong, "Effects of pre-strain on transformation temperatures of NiTi shape memory alloys", *Journal of Materials Science Letters*, **18**, pp. 1797-1798, 1999.
9. T. Tadaki, Y. Nakata, and K. Shimizu, "Thermal Cycling Effects in an Aged Ni-rich Ti-Ni Shape Memory Alloy", *Transactions of the Japan Institute of Metals*, **28**, No.11, pp. 883-890, 1987.
10. S.K. Wu, H.C. Lin, and T.S. Chou, *Acta metal. mater.*, **38**, pp. 95-102, 1990.
11. W. Huang, *Journal of Materials Science Letters*, **17**, pp. 1843-1844, 1998.
12. D. Goldstein, L. Kabacoff, and J. Tydings, "Stress Effects on Nitinol Phase Transformation", *Journal of Metals*, **39**, pp. 19-26, 1987.
13. Standard Test Methods of Tension Testing of Metallic Materials, Designation: E8-00, Annual Book of ASTM Standards, Vol. 3.0.1 (American Society for Testing and Materials, Philadelphia, PA, 2000), pp. 56-76.
14. Y. Liu, Z. Xie, J. Van Humbeek, and L. Delaey, "Asymmetry of stress-strain curves under tension and compression for NiTi shape memory alloys", *Materials Science and Engineering*, **A273-275**, pp. 679-684, 1999.
15. D.S. Ford and S.R. White, "Thermomechanical Behavior Of 55Ni45Ti Nitinol", *Acta mater.* **44**, pp.2295-2307, 1996.
16. S. K. Wu, H. C. Lin, Y. C. Yen, and J. C. Chen, "Wire drawing conducted in the R-phase of TiNi shape memory alloys", *Materials Letters*, **46**, pp.175-180, 2000.

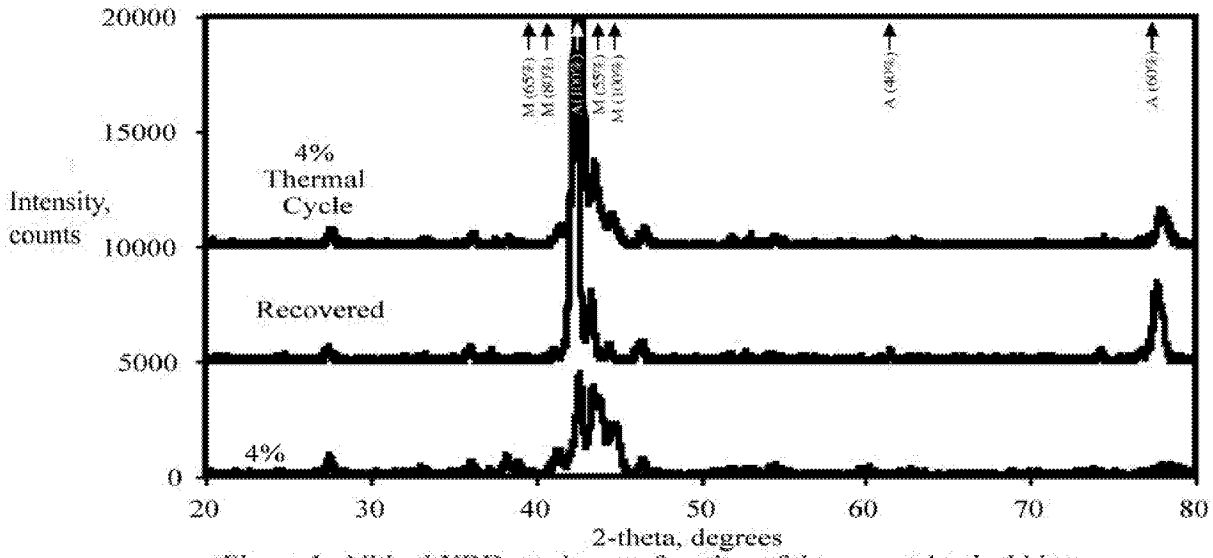

Figure 1. Nitinol XRD results as a function of thermomechanical history.

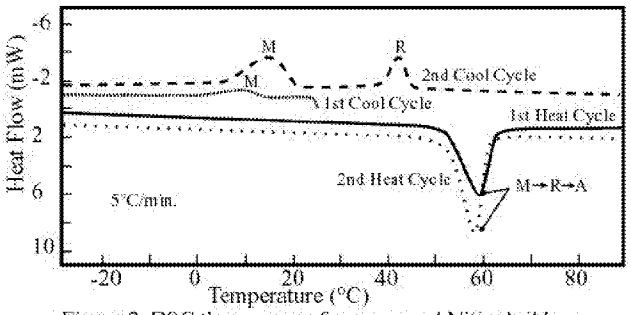

Figure 2. DSC thermogram for recovered Nitinol ribbon.

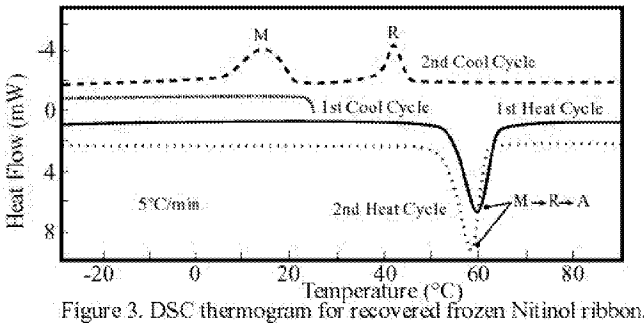

Figure 3. DSC thermogram for recovered frozen Nitinol ribbon.

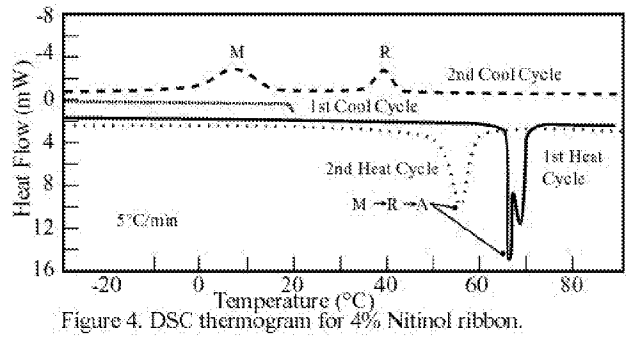

Figure 4. DSC thermogram for 4% Nitinol ribbon.

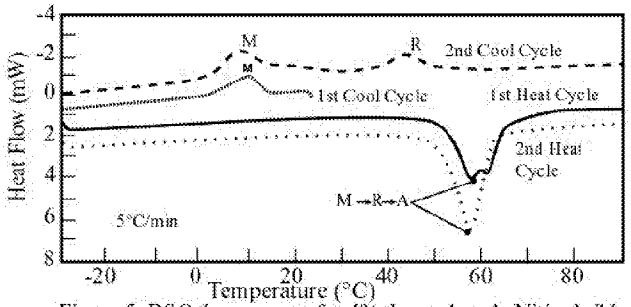

Figure 5. DSC thermogram for 4% thermal cycle Nitinol ribbon.

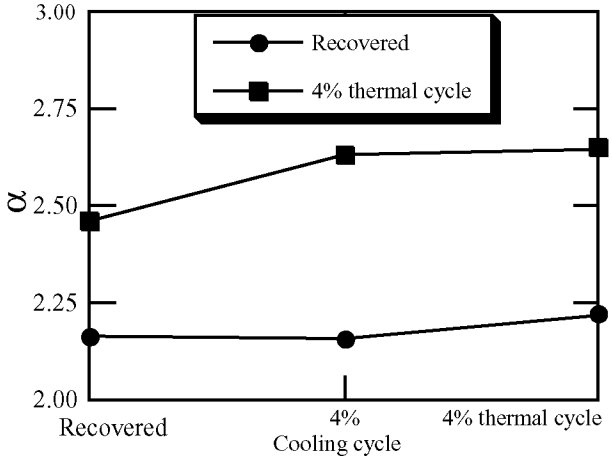

Figure 6. Variation of alpha with cooling cycle for the recovered and 4% thermal cycle conditions.

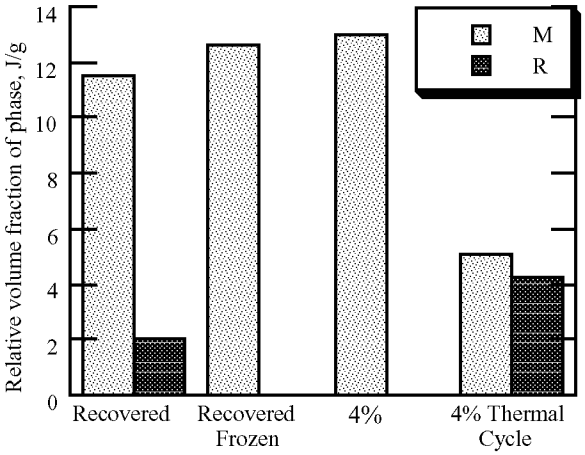

Figure 7. Relative volume fractions of martensite (B19') and R-phase in the ambient microstructure of the four alloy conditions based on DSC results.

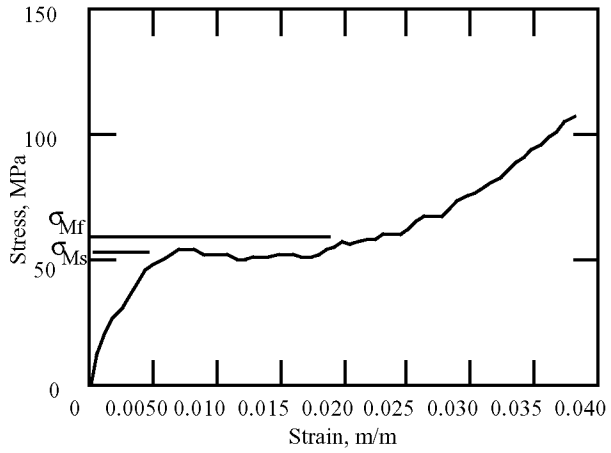

Figure 8. Stress-strain behavior of Recovered Nitinol ribbon during 4% pre-strain procedure.

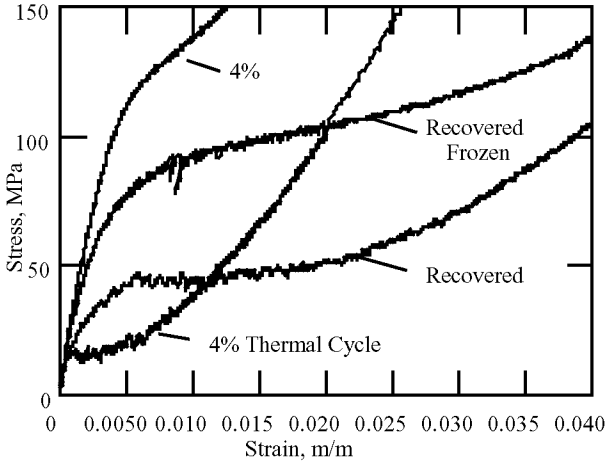

Figure 9 (a). Initial stress-strain behavior of Nitinol ribbons as a function of thermomechanical history.

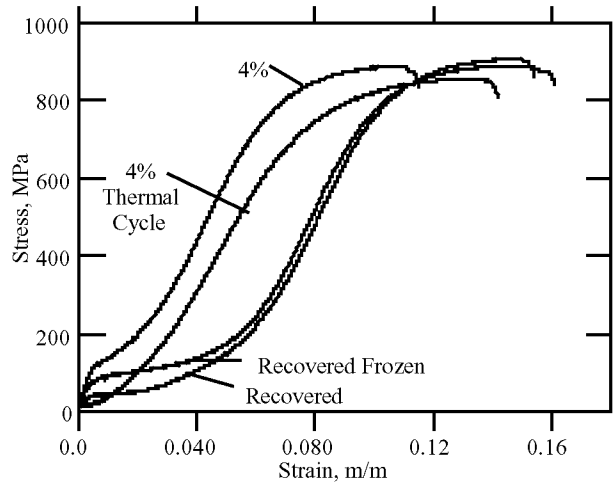

Figure 9 (b). Stress-strain behavior of Nitinol ribbons as a function of thermomechanical history.

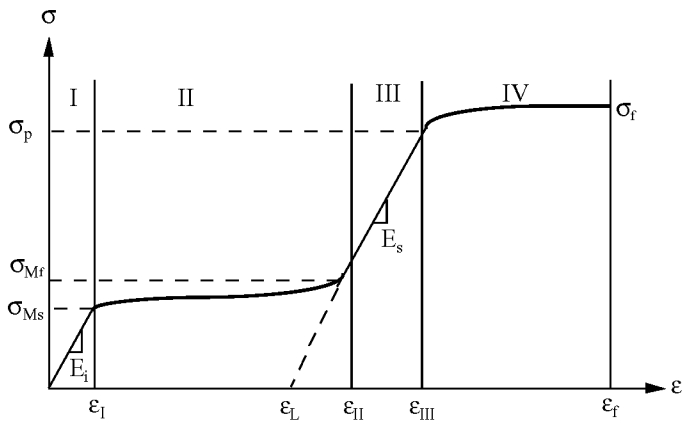

Figure 10. Idealized schematic of Nitinol stress-strain curve.